Development of immunotheranostic formulations based on Solid Lipid Nanoparticles

Erasmus Mundus Joint Master Degree in Surface, Electro, Radiation, & Photo Chemistry (SERP+)

By

Fabiana Dango

Supervisors:

Ana Hortelão

PhD

Manuel Bañobre-López

PhD

International Iberian Nanotechnology Laboratory

This page has been intentionally left blank

Table of contents

Abstract

Cancer is a leading cause of death worldwide, causing millions of deaths every year. The ability of cancer cells to elude the immune system is one of the aspects that make this illness difficult to defeat. Indoleamine 2,3-dioxygenase 1 (IDO1) is an enzyme that plays an important role in cancer immune evasion by decreasing tryptophan (Trp) and producing kynurenine metabolites which cloak the tumor from the immune cells. This work presents the development of immunotheranostic formulations based on solid lipid nanoparticles (SLNs) that combine non-invasive diagnostic imaging and therapeutic capabilities for IDO1 inhibition. The immunotheranostic formulations consist of a lipid matrix made of carnauba wax, encapsulating magnetite nanoparticles, and IDO1 small-drug inhibitors such as Indoximod, Epacadostat, and Linrodostat. The surface of the SLNs was functionalized with Trp to target solid tumors since several types of these cancers overexpress markers for Trp metabolism. The formulations were thoroughly characterized and showed high drug encapsulation efficiency (>98%) and ~ 60% drug release after 48 hours. The synthesized SLNs also demonstrated to be promising tools as T_2-contrast agents (transverse relaxivity value, r_2>130 $mM^{-1}s^{-1}$) and as heat generators for magnetic hyperthermia (specific absorption rate, SAR > 500 W/g). Therefore, the synthesized formulations are promising for application as theranostic tools in cancer immunotherapy.

Resumo

O cancro é uma das principais causas de morte a nível global, dando origem a milhões de mortes anualmente. A capacidade que as células cancerígenas têm de evitar o sistema imunitário é um dos fatores que torna tão difícil tratar esta doença. Indoleamina 2,3-dioxigenase 1 (IDO1) é uma enzima que desempenha um papel crucial na evasão do cancro ao sistema imunitário, uma vez que diminui a quantidade de triptofano (Trp) e aumenta a produção de metabólitos quinurenina que encobrem o tumor das células imunitárias. Este trabalho descreve o desenvolvimento de formulações imunoteranósticas baseadas em nanopartículas lipídicas sólidas (SLNs) que combinam um diagnóstico de imagem não-invasivo com as capacidades terapêuticas de inibidores de IDO1. As formulações imunoteranósticas são constituídas por uma matriz de lípidos feita a partir de cera de carnaúba que encapsulam nanopartículas de magnetite e inibidores da enzima IDO1, como a Indoximod, Epacadostat e Linrodostat. A superfícies das SLNs foi funcionalizada com Trp de modo a direcionar as formulações a tumores sólidos, uma vez que vários tipos de tumores superexpressão marcadores para o metabolismo de Trp. Estas formulações foram caracterizadas de modo extensivo e demonstraram elevada eficácia no encapsulamento de fármacos (>98%) e 60% de libertação do fármaco após 48 horas. As SLNs que foram sintetizadas também demonstram potencial como agentes de contraste T_2 (valor de relaxamento, r_2>130 Mm^{-1} s^{-1}) e como geradores de calor por hipertermia magnética (teste de absorção de energia, SAR > 500 Wg^{-1}). Concluindo, as formulações sintetizadas revelam se promissoras para aplicações teranósticas em imunoterapia orientada para o cancro**.**

Acknowledgments
Firstly, I would like to thank my supervisor, Dr. Ana Hortelão, for her support, and encouragement during my internship. Thank you for assisting me in the most challenging moments of the project and for allowing me to work independently, making it possible to develop my scientific and organizational skills. I would also like to thank my co-supervisor, Dr. Manuel Bañobre, for giving me this opportunity and for the guidance provided throughout my internship. Thanks to all the Nanomedicine Group at INL for the support shown in these six months. A special thanks goes to Ana Cristina Ribeiro, for her unconditional help during my internship. I also acknowledge the financial support of the project CiNTech, reference n.º C644865576-00000005, co-funded by Component C5 – Capitalisation and Business Innovation under the Portuguese Resilience and Recovery Plan, through the NextGenerationEU Fund.

A huge thank you to Nasrullah, who never stopped believing in me since I was in my undergraduate, and without whose guidance and wise advice I would not be here.

I am extremely grateful to the SERP+ Program and the European Commission for allowing me to study in an international and enriching environment.

To the SERP+ family, for being the best part of this adventure. Thank you for being a part of my journey towards becoming a better version of myself. Thank you for the long study sessions together, the even longer cactus and gossip sections, and the infinite laughs. Sharing these last two years with you has been an incredible and unforgettable experience. Thank you for the invaluable cultural exchange, for teaching me that pineapple does not grow on palms, and for cooking incredible dishes that I keep failing to recreate.

To the students who joined the SERP+ family, shared with us incredible moments, and supported us in our journey.

To all of you, you will be in my heart forever. Thank you for making this moment of my life full of happiness.

Finally, I would like to express my gratitude to my family for their education and support, without which I would not be the person I am today. Thanks to my little sister for always being that irrational, funny, and incredibly talkative person who makes me laugh all the time.

List of abbreviations

AC Alternating Current

ASTM American Society for Testing and Materials International

ATP Adenosine Triphosphate

AuNPs Gold Nanoparticles

DC Direct Current

DLS Dynamic Light Scattering

DMF N, N-Dimethylformamide

DPPE 1,2-Dipalmitoyl-sn-glycero-3-phosphoethanolamine

DPPE-SLNs@SPIONs SLNs containing the lipidic ligand DPPE

DPPE-Trp-SLNs@SPIONs Tryptophan-functionalized SLNs

EDC N-(3-Dimethylaminopropyl)-N'ethylcarbodiimide hydrochloride

EE% Encapsulation efficiency

FDA Food and Drug Administration

FTIR Fourier-transform Infrared Spectroscopy

HPLC High-performance Liquid Chromatography

ICIs Immune Checkpoint Inhibitors

ICP-OES Inductively coupled plasma-optical emission spectrometry

IDO1 Indoleamine 2,3-dioxygenase-1

IR Infrared

MEMS Multi-echo-multi-slice

MNs Magnetic Nanoparticles

MRI Magnetic Resonance Imaging

M_s Saturation Magnetization

NTA Nanoparticle Tracking Analysis

NPs Nanoparticles

PBMCs Peripheral Blood Mononuclear Cell

PBS Phosphate-buffered saline

PD-1 Programmed Death-1

PD-L1 Programmed Death Ligand-1

PI Polydispersity Index

PLGA Poly lactic-co-glycolic acid

r_2 Transverse Relaxivity

SLNs Solid Lipid Nanoparticles

SLNs@SPIONs SLN encapsulating SPIONs

SPIONs Superparamagnetic Iron Oxide Nanoparticles

TAMs Tumor-Associated Macrophages

TEM Transmission Electron Microscopy

TME Tumor Microenvironment

Treg Regulatory T-cells

Trp Tryptophan

XRD X-Ray Diffraction

1. Introduction

Cancer is generally defined as the uncontrolled growth of cells caused by the accumulation of genetic mutations.[1] It is a leading cause of death worldwide, with lung, breast, and colon cancer being the most diffused. According to the World Health Organization, nearly 10 million deaths were attributed to cancer in 2022.[2] Even though recent advances in medicine have allowed to improve the quality of life of people fighting against this illness, the most effective cancer treatments are still surgery and chemotherapy, which are invasive and provoke severe side effects.[3] While surgery can be used only for localized and accessible tumors, chemotherapy destroys cancer and healthy cells indiscriminately.[4] The non-specificity and toxicity of traditional cancer treatments, together with the increase in cancer incidence worldwide, make the development of new drugs necessary and urgent.[5]

However, the development of new treatments is hampered by the complexity of cancer biology. Among the hallmarks of cancer, genome instability, replicative immortality, resistance to cell death, induction of angiogenesis, and avoidance of the immune system are the features that make the spreading of abnormal cells fast and difficult to avoid.[6] These features, together with the heterogeneity of cancer biology, make the formulation of efficient, non-invasive, and fast methods for curing cancer challenging.

1.1. Immune system and cancer evasion

The immune system is a network of substances responsible for the detection and elimination of organisms harmful to the human body, called pathogens.[7] It is composed of innate and adaptive immune cells. The innate immune system is composed of macrophages, dendritic cells, and natural killers. They provide a fast and non-specific response to pathogens, while the adaptive immune system, consisting of T-cells and B-cells, provides an antigen-specific response and is responsible for the memory of the immune system.[7,8] Immune cells are responsible not only for the elimination of external pathogens but also for the recognition of abnormalities in normal tissues.[7] Hence, they play an important role in the identification and removal of cancer cells, which normally express tumor-associated antigens and are thus recognized and eliminated by the immune system.[4,9] Despite the expression of immunogenic antigens, however, cancer is still able to evade immune system, thanks to the intricate complexity of the tumor microenvironment (TME).[9,10] The penetration of immune cells into the tumor is obstructed by the characteristics of the TME. The hypoxic state found in cancer cells inhibits immune signals and hinders the penetration of the T-cells.[4,11] On the other side, the high oxidative stress state of the cancer cells influences the functioning of natural killers and dendritic cells, making them less efficient. Furthermore, cancer is able to regulate the immune system in different ways, such as through the expression of specific antigens. Cancer cells can avoid elimination by T-cells through the expression of Programmed Death Ligand-1 (PD-L1), which binds the Programmed Death-1 (PD-1) found on the surface of natural killer cells and T-cells, making them ineffective. PD-L1 can be overexpressed also on the surface of tumor-associated macrophages (TAMs), which are normally specialized in the elimination of abnormal cells. Furthermore, among the most effective ways used by cancer cells to inhibit T-cells, is the regulation of tryptophan catabolism. Tryptophan is an essential amino acid metabolized to kynurenine in the kynurenine pathway.[12] The first step of the kynurenine pathway is catalyzed by an enzyme called Indoleamine 2,3-dioxygenase-1 (IDO1), whose important role in cancer was observed for the first time in 1950.[10,12] However, the role of IDO1 in mediating immunosuppression was made clear only in 1998 by Munn and Mellor, who discovered the influence of Tryptophan (Trp) deprivation on T-cells.[10] The overexpression of IDO1 in cancer was found to be associated with immune escape and inefficiency of T-Cells.[12] When IDO1 is overexpressed, Trp is converted to kynurenine at a higher dose than in normal conditions. This causes Trp deprivation in cancer cells, to which T-cells are sensitive.[10,12] At the same time, it can cause a higher production of regulatory T-cells (Treg), which normally suppress T-cells in order to avoid autoimmune responses.[11] Hence, the regulation of the immune system by

cancer is an important aspect of its progression. Understanding the mechanisms used by cancer cells to evade the immune system can provide useful insights for alternative treatments.

1.2. Cancer immunotherapy

Due to the discovery of immune system evasion by cancer, several studies have been conducted to enhance the immune activity of cancer, leading to the discovery of a new therapeutic approach, called immunotherapy. [4,8,13] Cancer immunotherapy is a treatment whose goal is to activate the immune system of the patient and cause the elimination of cancer cells. It uses a different approach compared to traditional cancer therapies, focusing on the activation of the immune system rather than on the elimination of cancer cells.[8,13] Immunotherapy is a promising treatment, as its goal is the activation of T-cells, which would be able to eliminate not only the primary tumor but also the metastasis.[11] Furthermore, the immune response caused by the immunotherapeutic agents should be selective for cancer cells, hence, it should not damage healthy tissues, unlike traditional therapies. Moreover, once the immune system has been activated, the antigens present on the cells of the adaptive immune system would avoid the formation of metastasis, acting in a preventive way.[13]

Despite the enormous potential, immunotherapy nowadays is still limited by some non-neglectable side effects. The activation of the immune system in an uncontrolled way, the low response of some tumors, and the complexity of the immune system are an obstacle in the formulation of efficient and selective drugs.[4,14] Furthermore, most of the FDA-approved immunotherapy formulations are biologics, such as antibiotics and oncolytic viruses.[15,16] Biological therapeutics still have some major drawbacks such as high cost of production and complex logistics for transportation and storage. At the same time, they showed low oral bioavailability and low uptake by the tumor.[17]

As an alternative to the employment of antibodies, small molecules have been proposed as a less expensive and toxic alternative.[11] Small molecules, compared to antibodies, can penetrate the tumor more easily and show better oral bioavailability. Their shorter half-life contributes to lowering their toxicity, and their size makes them eligible for intracellular and extracellular targets.[11,17] Many small molecules have proved to be efficient and reached clinical trials, such as Imiquimod, which reached Phase III in metastatic melanoma, Resiquimod, which reached Phase II for brain tumors, and ADU-S100, which reached Phase II in recurrent and metastatic head and neck squamous cell carcinoma.[11,17]

1.3. Small molecules as IDO1 inhibitors

Small molecules have been employed also for the inhibition of IDO1 and reached clinical trials proving their efficacy.[17] Indoximod was the first small molecule employed in humans for the inhibition of IDO1 activity.[11] Indoximod is the commercial name for 1-Methyl-D-tryptophan, a small molecule able to act as an inhibitor of IDO1, promoting the production of T-cells and decreasing the proliferation of Tregs.[11,18] Indoximod proved to have a beneficial effect on the complex mTORC1, which is inhibited when IDO1 is overexpressed resulting in a decrease in the function of the T-cells. Indoximod can activate mTORC1, reactivating T-cells to fight cancer.[10] It reached clinical trials, was well tolerated in Phase 1 and was safe up to 2000 mg twice/day.[10,17] In Phase II it was administered with pembrolizumab, a PD-1 antibody, and reached positive results in patients with melanoma.[10,17] Another efficient IDO1 inhibitor is Epacadostat, which reached Phase III trial in combination with pembrolizumab for melanoma treatment.[17] Epacadostat contains an important functional group, the hydroxyamidine, able to bind to the iron of the heme group of IDO1, inhibiting its effect. Thus, Epacadostat is a strong inhibitor of IDO1, able to restore the proliferation of T-cells and natural killer cells and inhibit the production of Tregs.[10] BMS-986,205 (Linrodostat), on the other side, demonstrated better pharmacokinetics compared to Epacadostat, and it was well tolerated in patients with doses up to 100 mg per day, in combination with Nivolumab.[10,19]

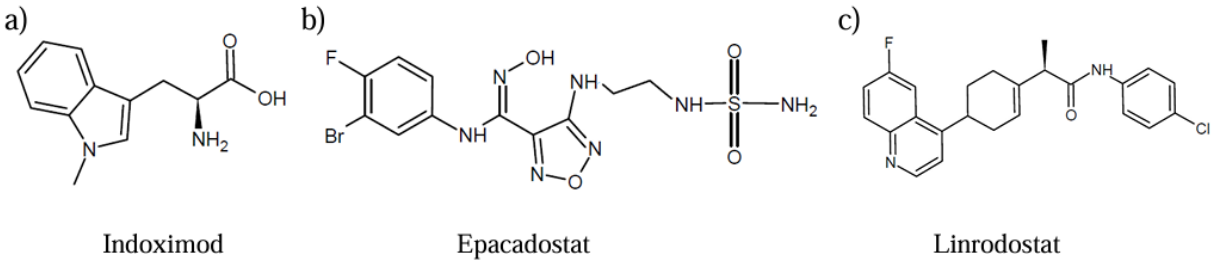

Figure 1: molecular structure of IDO1 inhibitors. a) Indoximod; b) Epacadostat; c) Linrodostat

However, the administration of free molecules is often associated with fast elimination and poor biological barrier crossing, which reduce the efficacy of treatments.[20] Furthermore, cancer immunotherapies are responsible for severe side effects, which could be life-threatening. In particular, the uncontrolled activation of the immune system and inflammatory response limited the translation of immunotherapies in clinical applications.[15,21] The use of drug delivery nanosystems has thus been explored as a mean to overcome these challenges.[20]

1.4. Nanoparticles for delivery of small molecules

In the past years, numerous drug delivery systems have been proposed to improve the therapeutic effect of anticancer drugs.[22] In the field of drug delivery systems, the employment of nanotechnology proved to be efficient in improving the toxicity profile, bioavailability, and circulation time of drugs.[8] Different kinds of nanoparticles (NPs) have been formulated, such as polymeric, inorganic, and lipid-based nanoparticles.[20] Polymeric NPs are widely used as drug delivery systems due to their biocompatibility. Poly lactic-co-glycolic acid (PLGA) NPs have been used to deliver anticancer vaccines, demonstrating that their encapsulation enhanced the targeted delivery and efficiency of the treatment.[8,20] Inorganic NPs such as gold NPs (AuNPs) and silica NPs have been employed in cancer treatment, showing high tumor uptake.[23] The most commonly used drug delivery systems are lipid-based NPs. Lipid-based NPs are in general spherical, biocompatible, able to encapsulate hydrophilic and hydrophobic compounds. Many formulations based on lipids have already been approved by the FDA.[20] Among the lipid-based nanoparticles, particular attention has been gained by solid lipid nanoparticles.[24]

1.5. Solid Lipid Nanoparticles (SLNs)

Among the different drug delivery systems developed for the transportation of anticancer drugs, the SLNs proved to be an efficient, easy-to-prepare, and stable nanocarrier.[25] SLNs are formed by a solid lipid core, called matrix, covered by a surfactant layer, that improves its stability in aqueous solutions. They are generally in the form of round nanoparticles, with hydrodynamic diameters comprised between 40 and 1000 nm.[26,27] Among the advantages of SLNs, is the possibility of encapsulating both hydrophobic and hydrophilic drugs, allowing efficient protection and transport in the bloodstream. Furthermore, they are composed of biodegradable substances, hence less toxic than other nanoparticles.[27] SLNs are therefore an efficient drug delivery system, which showed sustained drug release profiles, is easily adaptable to production on a large scale, and does not use organic solvents.[26,27] The production of SLNs can be obtained using different methods such as high-shear homogenization, high-pressure homogenization, emulsion, and ultrasonication.[28–30] The principle of the synthesis methods of SLNs is the agitation of the mixture in the presence of a surfactant. The presence of the latter is important as it can reduce the interfacial tension between the two liquids, forming stable SLNs.[30] Furthermore, lipid nanoparticles can be functionalized.[26] This is particularly important for drug delivery systems as one of the main limitations of traditional nanocarriers is their non-specificity.[4] Hence, nanomedicines used in the field of immunotherapy, still face some challenges due to the side effects produced on healthy cells. Nano-

formulations with a functionalized surface could enhance the penetration in the tumor and minimize side effects.[4]

1.5.1. SLNs for cancer theranostics

As SLNs are typically biocompatible and safe, they are good candidates for cancer theranostics.[31] Theranostics is a recent approach, whose goal is integrating in the same particle diagnostic/monitoring and treatment capabilities. The image obtained from the nanoparticle allows tumor visualization and monitoring over time. At the same time, the therapeutic agent encapsulated is released and allows the shrinkage of the tumor.[32] The controlled and targeted release maximizes the efficacy of the treatment.[31,32] Theranostics aims at detecting and effectively curing cancer using a single non-invasive formulation. Examples of imaging techniques are ultrasound, magnetic resonance imaging (MRI), optical fluorescence, and bioluminescence.[31,32]

However, nanotheranostics formulations, so far, have been scarcely translated into clinics, mainly due to concerns regarding their efficacy, safety, and biocompatibility. The synthetic complexity is also contributing to the difficulty in scaling up the process in a green manner.[31,33]

1.6. Nanoparticle characterization techniques

Nanoparticles should be characterized both in terms of physical and chemical properties and in terms of functional properties. For the former, size, surface charge, morphology, chemical composition, and crystallographic structure of the components are key parameters to be assessed: *size* can be characterized using techniques such as dynamic light scattering (DLS) or nanoparticle tracking analysis (NTA), which allow the determination of the hydrodynamic diameter of the particles; *surface charge* is also determined using DLS; in turn, the *morphology* of the nanoparticles is evaluated using transmission electron microscopy (TEM). The *composition* of the nanoparticles can be studied using Fourier-transform infrared spectroscopy (FTIR), while Inductively Coupled Plasma (ICP) spectroscopy is utilized for the *quantification* of the elements present in the nanoparticle; in turn, the determination of the *crystallographic structure* is possible using X-Ray diffraction (XRD). *Drug encapsulation and release* are determined using High-performance liquid chromatography (HPLC). For the latter, an analysis of nanoparticles' magnetic properties is required. The *magnetic behavior* can be analyzed using vibrating sample magnetometry (VSM); the *heating capability* of the sample is determined using magnetic hyperthermia (MH); in turn, magnetic resonance imaging (MRI) is suitable for studying the contrast enhancement capability of the formulations.

1.6.1. Dynamic light scattering

DLS is a characterization technique used to determine the particle size, size distribution, and ζ-potential. Measurements of the particle size and size distribution are carried out by measuring changes in the scattered light due to Brownian motion.[34] A monochromatic light irradiates the sample and the scattered light is collected by a detector. Small particles diffuse faster, while large particles diffuse slower, provoking a slower fluctuation in scattered light. DLS provides an autocorrelation function, where the faster the decay, the smaller the particles. From the Stokes-Einstein equation (Equation 1) it is possible to calculate the hydrodynamic radius (R_h) of the nanoparticles, using the diffusion coefficient obtained from the autocorrelation function.

$$D_\tau = \frac{\kappa_B T}{6\pi\eta R_h} \quad (1)$$

Where D_τ is the diffusion coefficient, κ_B is the Boltzmann constant, T is the temperature, and η the viscosity of the solvent.

The ζ-potential, on the other side, cannot be measured directly. ζ-potential is defined as the potential developed at the interface between the nanoparticles and the medium in which they are dispersed when a potential is applied to the solution. It is calculated from the electrophoretic

mobility, which is the ratio between the velocity of the particles and the electric field strength, using Equation 2.

$$\mu_e = \frac{2\varepsilon_r \varepsilon_0 \zeta f(Ka)}{3\eta} \quad (2)$$

Where ε_r is the dielectric constant, ε_0 is the permittivity of vacuum, f(Ka) is the Henry's function and η is the viscosity.[35]

1.6.2. Nanoparticle Tracking Analysis

An alternative method for analyzing the size of nanoparticles is NTA, which is a technique that analyses the Brownian motions, similarly to DLS, of nanoparticles with a size comprised between 30 and 1000 nm.[36] As in the DLS, a laser beam irradiates the sample and is scattered in all directions. A light-sensitive camera placed at 90° from the incident beam collects the scattered light and the scattering of the particles is visible using a specific software.[37] Using NTA it is possible to correlate particle movement with their size by using a variation of Equation 1, where the Dτ is obtained from the mean velocity of the particles using Equation 3.[36]

$$D = \frac{\overline{(x,y)^2}}{4t} \quad (3)$$

1.6.3. Transmission electron microscopy

TEM is a technique widely used to analyze the morphology of materials on the nanoscale.[38] A TEM microscope is composed of an electron gun, lenses that focus the electrons, and a detector. The electron gun accelerates electrons with a voltage in the range of 80kV to 300kV. The accelerated electrons are focused on the sample by the condenser lenses, and they can pass through the sample, which is positioned in a holder. The transmitted electrons are focused on the detector by another set of lenses, where they form an image. TEM is widely used because of the very high image resolution which allows the visualization of details in atomic scale. However, it is a technique that uses a vacuum to avoid scattering of the electron from the electron source to the sample, and the high energy of the electrons could damage the sample, especially in the case of polymers, biological, or organic samples. Techniques such as Cryo-TEM, which allows to visualize biological samples using ultra-fast cooling, have been developed to avoid damaging the sample.[39]

1.6.4. Fourier-transform infrared spectroscopy

FTIR is a technique used to identify the functional groups of molecules, based on their interaction with infrared (IR) radiation. The sample absorbs infrared light, which causes transitions in the ground state's vibrational and rotational energy levels. The transmitted light is collected by a detector and the signal is converted into an IR spectrum using Fourier transformation. The transmittance versus wavenumber is plotted, and the functional groups are identified based on the position of the absorption bands.[40]

1.6.5. X-ray diffraction

In an XRD experiment, an X-ray beam is directed toward the sample and is scattered in all directions by the atoms. However, only the constructive scattered radiation will create a signal. The conditions for constructive interference are determined by Bragg's law (Equation 4)

$$n\lambda = 2dsin\theta, \quad (4)$$

where n is the order of diffraction, λ is the wavelength (nm), d is the lattice spacing (nm) and θ is the angle of the diffracted beam (°). The diffracted beam is collected by a detector and the intensity versus 2θ is plotted. The position of the peaks allows the identification of the material.[41]

1.6.6. Magnetic Resonance Imaging

MRI is a technique widely used in medicine for diagnosis and monitoring of treatments. It is based on the principle that water protons surrounded by different environments will give different contrast images. A strong magnetic field is applied and the nuclear spins of the hydrogen atoms of water molecules align with it. A radiofrequency is then applied to disturb the alignment. When the nuclei relax back to their equilibrium state they emit a signal, which is collected by a detector and analyzed to obtain images of tissues.[42]

1.6.7. High-performance Liquid Chromatography

HPLC is a technique widely used for the identification and quantification of components of a sample.[43] The sample mixture is pumped into a column, made of a solid material, at high pressure. The sample mixes with the mobile phase, and different components will pass through the column at different rates. The signal is analyzed by a detector and the absorbance versus retention time is plotted in a chromatogram.

1.6.8. Inductively coupled plasma-optical emission spectrometry (ICP-OES)

ICP-OES is a technique used to quantify trace elements in the sample. The liquid sample is first converted into an aerosol spray and then passes through a hot plasma.[44] Here, the elements are excited, and light with characteristic wavelengths is emitted. This light is analyzed using a spectrometer, and the intensity gives information about the concentration of the element in the sample.

1.6.9. Magnetometry

The magnetic behavior of the materials can be studied using magnetometry. A *vibrating sample magnetometer* is used to measure the magnetic properties of the material as a function of the temperature and magnetic field.[45] The magnetic moments of the sample align with the supplied magnetic field. As the sample vibrates, the magnetic field changes and it is detected by the coils. The alternating magnetic field produced by the sample will generate a current, which increases with increasing magnetization. From VSM it is possible to obtain information about the magnetic saturation and coercivity of the material, which determine its magnetic state. Instead, *alternating current (AC)* magnetometry is used to obtain the sample's specific absorption rate (SAR), which is the amount of heat generated per gram of the magnetic nanoparticle in a given time.[46] It consists of the generation of an alternating magnetic field and the detection of the sample's response through a coil. From AC magnetometry it is possible to obtain hysteresis loops by plotting the magnetization versus the applied magnetic field. The area of the hysteresis loop is directly proportional to the SAR value.[47]

1.6.10. Inductive heating

Inductive heating is a technique used to generate heat starting from electromagnetic energy using magnetic nanoparticles.[48] Magnetic nanoparticles can produce magnetic energy when subject to an alternating magnetic field. The magnetic energy is then converted into heat. From the variation of temperature with time it is possible to calculate the SAR value using Equation 5

$$SAR = \frac{C_{H_2O}}{m_{Fe}} \cdot \frac{dT}{dt}, \quad (5)$$

where C_{H_2O} is the specific heat capacity of water (4.185 $Jg^{-1}°C^{-1}$), m_{Fe} is the mass of iron per gram of sample and dT/dt is the slope of the initial temperature vs time curve.

1.7. Objectives of the study

The aim of this work is the development of immunotheranostic magnetic formulations based on SLNs, with immuno-modulating properties, the capability of targeting tumors, and functional theranostic performance including magnetic hyperthermia and magnetic resonance imaging capabilities. For this, we divided the work into three main objectives: *i)* synthesis and characterization of different immunotheranostic SLNs prototypes of increasing levels of complexity; *ii)* evaluation of the encapsulation efficiency and release kinetics of immunomodulator drugs; *iii)* characterization of the functional properties of the immunotheranostic SLNs and assessment of their effect on cell viability.

2. Material and Methods

2.1. Materials

Tween® 80, L-Tryptophan (99.5%), 1,2-Dipalmitoyl-sn-glycero-3-phosphoethanolamine ≥97% (DPPE), N-(3-Dimethylaminopropyl)-N'ethylcarbodiimide hydrochloride (EDC), N, N-Dimethylformamide (DMF) (99.8%), Iron(II) chloride tetrahydrate (>99.0%), Iron(III) chloride hexahydrate (>99.0%), trifluoroacetic acid (≥99%), and Triton X-100 (1%) were purchased from Sigma-Aldrich. Carnauba wax T1 flakes were purchased from Koster Keunen Holland BV. Hydrochloric acid (37%), chloroform (99.8%), Diethyl ether (99.5%), oleic acid, Dulbecco's Modified Eagle Medium (DMEM), Roswell Park Memorial Institute Medium (RPMI) were purchased from Thermo Fisher Scientific. Ammonia solution (30%), acetonitrile HPLC grade were purchased from LabChem. 1-Methyl-D-tryptophan (>98%), BMS-986205, INCB024360, were purchased from AdooQ Bioscience. AquaBluer reagent was purchased from MultiTarget Pharmaceuticals LLC.

2.2.Equipment

The synthesis of SLNs was performed using Branson Ultrasonic Disintegrator Mod. 450. The Metabo HE 20-600 hot air gun was used during the experiment to heat the sample. The nanoparticles were characterized using DLS, NTA, and TEM. Hydrodynamic sizes were determined using Anton Paar Litesizer DLS 500 and Malvern Panalytical NanoSight NS300. TEM images were captured using a JEOL JEM-2100 microscope at an accelerating voltage of 200 kV. The iron concentration in the SLNs and SPIONs was measured using a Shimadzu ICPE-9000 Multitype ICP Emission Spectrometer and the presence of Iron in magnetite form was confirmed using Panalytical X'Pert Pro MRD X-Ray Diffractometer. For testing the yield of the fuctionalization reaction, the Horiba FluoroMax-4 Compact Spectrofluorometer was used. The SLNs were further characterized using Bruker Vertex 80v vacuum Fourier Transform Infrared (FTIR) Spectrometer. The magnetic properties of the SLNs were studied using a DM 100 System from nB Nanoscale Biomagnetics (hyperthermia) and a 3.0 T horizontal bore MR Solutions Benchtop MRI system equipped with 48 Gcm^{-1} actively shielded gradients. The drug encapsulation and release were analyzed using a UHPLC Agilent 1290 Infinity II LC System and a Tracer Excel 120 ODSB 5µm column. Drug release in hyperthermia was performed using a NAN201003 Magnetherm from NanoTherics. AC magnetometry was performed using the AC Hyster™ Series magnetometer from Nanotech Solutions. DC magnetometry was performed using a vibrating sample magnetometer 3473-70 L.O.T.-Oriel.

2.3. Superparamagnetic Iron Oxide Nanoparticles Synthesis

In a beaker, 46.3 mmol of $FeCl_2 \cdot 4H_2O$ and 55.6 mmol of $FeCl_3 \cdot 6H_2O$ were dissolved in 250 ml of milli-Q water and stirred for 10 minutes at 50 °C. Dropwise, 21.1 mL of NH_4OH (30% v/v) were added causing the formation of a black precipitate. The solution turned black and 2.5 mL of oleic acid were added. The solution was heated at 80 °C for one hour. After reaction completion, the magnetic nanoparticles (MNs) were separated magnetically, and the solution was washed

twice with milli-Q water to remove the excess of solvent. To remove the water, the MNs were washed twice with a solution of hexane and ethanol and allowed to dry overnight. The MNs were then dissolved in the minimum amount of chloroform and stored in the fridge.

2.4. Characterization of SPIONs

SPIONs morphology was analyzed using TEM images. The chloroform dispersion was placed onto a carbon-coated Cu-grid and the solvent evaporated overnight. The iron concentration was determined using ICP-OES. 1 µL of the dispersion in chloroform was diluted in 999 µL of HCl (37% v/v) and digested overnight. Milli-Q water was added to obtain a final volume of 12 mL, and the sample was filtered using a 220 nm sterile PES syringe filter. The presence of magnetite was confirmed by XRD analysis. The chloroform dispersion of SPIONs was placed on the holder and allowed to evaporate. The procedure was repeated until the holder was completely covered by a black uniform layer.

2.5. Targeted theranostics SLNs Synthesis

Control SLN were synthesized by mixing 200 mg of Carnauba with 0.5 mL of an aqueous solution (50 mg/mL) of tween 80® and 4.5 mL of milli-Q water which were previously heated at 80 °C on the hot plate. The solution was then heated with a heat gun until all the wax was melted and separate liquid organic and aqueous layers were visible. Once the wax melted, the solution was sonicated for 2 minutes at 20 s ON/OFF cycles. During sonication, the heat gun was employed to keep the sample warm. Once the procedure was complete, the vial was rapidly closed and placed in an ice bath. To separate the unreacted compounds, centrifugation was used. The samples were centrifuged at 1811 rcf for 10 minutes. A small quantity of sediments was observed, and the supernatant was transferred into vials for further studies. In turn, SLN encapsulating SPIONs (*SLN@SPIONs*) were synthesized using roughly the same procedure, with the exception that the SPIONs dispersion in chloroform (containing 40 mg of Fe_3O_4) was added to the wax in the glass vial and the chloroform was evaporated overnight before initializing the synthesis. The SLN containing the lipidic ligand DPPE (*DPPE-SLN@SPIONs*) prototype was synthesized via the same route, evaporating both the SPIONs dispersion and 0.5 mL of the chloroform solution of DPPE (10 mg/mL) overnight prior to the synthesis. Finally, the tryptophan-functionalized SLN (*DPPE-Trp-SLN@SPIONs*) was synthesized using the same protocol, with the addition of SPIONs dispersion (containing 40 mg of Fe_3O_4), and 1.79 mL of the chloroform solution of functionalized DPPE (2.8mg/mL) and evaporation overnight.

2.6. Functionalization of lipidic ligand DPPE

The lipidic ligand DPPE was functionalized with Trp via two routes. In both procedures, an EDC-NHS reaction was performed. The first approach (approach 1) consisted of the functionalization of DPPE with Trp prior to its incorporation in the SLN, and the second procedure (approach 2) involved performing the synthesis of the SLN containing bare DPPE first and functionalizing the lipidic ligand with Trp after the SLN synthesis. *Approach* 1: For the functionalization of DPPE before the synthesis of the SLN, in a round bottom flask, L-Trp (0,0505 mmol) was dissolved in DMF (25 mL). The solution was sonicated at 40 °C and 37 kHz for 10 minutes to promote the solubilization of Trp. After, 1.1 eq. of EDC was added. Following 30 minutes of stirring at RT, 1.1 eq. of NHS was added. After 30 minutes, 2 eq. of DPPE were added. The solution was sonicated for 5 minutes at 40 °C and 37 kHz and stirred overnight. After this, diethyl ether was added to the round bottom flask to precipitate the lipid, and the mixture was placed at 4 °C. Once a white layer of precipitate lipid was visible in the bottom of the flask, the solvent was carefully separated from the lipid. The leftover solvent was evaporated using nitrogen gas. The remaining lipid was dissolved in the smallest amount of chloroform and stored at 4 °C. *Approach* 2: For the functionalization of the DPPE after the SLN synthesis, 5 ml of an aqueous solution containing 180 µmol of Trp was placed in a flask with 1.1 eq. of EDC and stirred for 30 minutes. 1.1 eq. of NHS were added and the reaction was carried out for 30 minutes. Following the reaction with

EDC and NHS, 5 ml of the previously synthesized DPPE-SLNs@SPIONs were added and the solution was stirred overnight. 1 ml of the solution was purified using centrifugal amicon filters (30 kDa) for 20 minutes at 14000 rcf. The unreacted reagents were separated from the SLNs using a dialysis kit Pur-A-Lyzer Midi^{TM} 3500. The water was exchanged every 2 hours for a total of 8 hours and then the sample was left dialyzing overnight.

2.7. Characterization of DPPE functionalization

Fluorescence detection. To calculate the yield of the reaction, the free Trp in solution was quantified. To quantify the Trp, fluorescence detection (λ_{ext}=280 nm, λ_{em}=350 nm) was performed. For approach one, after precipitating the lipid, an aliquot of the remaining solvent was analyzed and the concentration of free Trp was determined. For approach 2, the purified solution was used for Trp quantification. The intensity of emission was correlated to the Trp concentration, and the yield of the reaction was calculated.

Hopkins-cole test. To prove the presence of Tryptophan in the functionalized lipid and in the SLNs, the Hopkins-Cole test was performed. 1 mL of a 0.1 M solution of glyoxylic acid was mixed with i) 2 mL of a chloroform solution of DPPE (1.5 mg/mL), as the negative control, ii) 1 mL of the chloroform solution of DPPE-Trp (2.8 mg/mL), iii) 3 mL of the DPPE-Trp-SLNs, iv) 3 mL of an ethanol solution of Trp (1 mg/mL), as the positive control. Sulfuric acid (98% v/v) was added dropwise to the vials, which were left in the hood until the completion of the reaction.

2.8. Physico-chemical characterization of targeted theranostics SLNs

The physical and chemical properties of the synthesized SLN were evaluated using different and complementary techniques. *Hydrodynamic diameter*: the size of the nanoparticles was determined using DLS and NTA. DLS was used to determine the hydrodynamic diameter, polydispersity index (PI), and ζ-potential. For this, the SLN dispersion was diluted in water (1:1000) and analyzed using a carbon electrode cell, using an Anton Paar Litesizer DLS 500 equipped with a 658 nm laser, and using a 173° detection angle. NTA was performed to corroborate the results obtained by DLS. A dilution (1:2000) in water was analyzed by static measurements, using a Malvern Panalytical NanoSight NS300 equipped with a 488 nm laser. *SLN Morphology*: the size and shape of the SLNs was analyzed using TEM. A dilution (1:10) in water of the SLN dispersions was prepared, 10 µL were deposited onto a carbon-coated Cu-grid and allowed to dry overnight. The JEOL JEM-2100 microscope uses a LaB6 electron gun and 4k x 4k CCD camera that operates at 25 fps. The *Fe concentration* was determined using ICP-OES, for this, 5 µL of the sample were dissolved in 995 µL of HCl (37% v/v) and allowed to digest overnight. Milli-Q water was added to obtain a final volume of 12 mL, and the sample was filtered using a 220 nm sterile PES syringe filter. *Incorporation of the DPPE ligand and Trp:* the presence of DPPE and Trp was studied using FTIR. The mixture containing SLNs was first dried using lyophilization. A small amount of the dried sample was used to perform FTIR analysis.

2.9. Immunomodulating Drug loading into SLNs

The drug-loaded SLNs were obtained by repeating the same procedures described in 2.5, but with the addition of different lyophilized drugs in the vial. The *SLNs@Indoximod* was synthesized with the addition of 40 mg of Indoximod. For the synthesis of *SLNs@Epacadostat,* 1 mg of the drug was added to the vial, while for the synthesis of *SLNs@Linrodostat* 5 mg of the drug were used. For the determination of drug loading, after the synthesis, 500 µL of the mixture containing SLNs@drug was purified using centrifugal amicon filters (30 kDa) for 20 minutes at 14 000 rcf. The drug encapsulation efficiency was then quantified was by HPLC using a gradient of water: acetonitrile (from 100% to 25:75%). UV (280 nm) was used for the detection of the peaks of the immunomodulating drugs.

2.10. *In vitro* drug release assays

The drug release was performed in physiological mimicking conditions (in Phosphate-buffered saline (PBS) + 1% Tween® 80, pH of 7.4) at 37°C up to 48 hours. 200 µL of the release medium were taken every 30 minutes for 5 hours, and then every hour, replenishing with 200 µL of fresh medium. Drug release in hyperthermia was performed in the same conditions, but applying an alternating magnetic field for 4 hours, taking samples for analysis every 30 minutes, and replenishing with fresh medium. The samples were then analyzed by HPLC, using the same method described in 2.9.

2.11. Magnetic characterization of theranostics SLNs

AC magnetometry was performed placing 40 µL of different SLNs containing SPIONs in the test tube and inserting it in the magnetometer. The frequency was kept constant at 300 kHz and the magnetic field amplitude was tuned between 4 kA/m and 24 kA/m. Hysteresis loops were recorded by plotting the magnetization versus applied magnetic field and SAR values were calculated from the area of the hysteresis loop. For the *inductive heating* studies, a vial containing 500 µL of the SLNs@SPIONs, DPPE-SLNs@SPIONs, and DPPE-Trp-SLNs@SPIONs was positioned in the middle of a copper coil cooled by water. A magnetic field of 200 Oe and an applied frequency of 869 kHz were applied for 1 hour. SAR values were determined using Equation 5. The first 50 s after the application of the magnetic field were used for the linear fitting of the temperature versus time curve, and SAR was calculated using the initial slope method. *Magnetic resonance imaging studies* were performed for the SLNs@SPIONs, DPPE-SLNs@SPIONs, and DPPE-Trp-SLNs@SPIONs. 100 µL of a solution containing increasing iron concentrations (10, 25, 50, 75, and 100 µM) were placed into the holder and placed at the center of the coil. Multi-echo-multi-slice (MEMS) sequences were recorded and T_2 maps were obtained using Image J. T_2-maps were used to obtain representative images of MRI contrast's capability dependence on iron concentration and relaxivity values. The relaxivity value (r_2) is the slope of the inverse of the transverse relaxation time versus iron concentration.

2.12. Cell studies

Cell viability studies. The effect of the different SLNs developed in this MSc project on cell viability was tested in different cell types: triple-negative breast cancer cell line (Hs578T), pancreatic cancer cell line (MIA-PACA-2), human dermal fibroblasts, as well as peripheral blood mononuclear cells (PBMCs). For this, the cells were seeded in flat bottom 96-well plates. Hs578T, MIA-PACA-2, and dermal fibroblast were seeded at a density of $1x10^4$ cells per well (in DMEN culture medium), while the PBMCs were seeded at a density of $5x10^4$ cells per well (in RPMI culture medium). The cells were then allowed to grow for 24 hours. After, SLNs at a range of concentrations (1.875, 3.75, 7.5, 15, 30, 60, 120 µg/mL) were added to the cells medium, and the cells were further incubated for 48 hours at 37 ºC, 5% CO2. The cell viability was then assessed using the AquaBluer reagent, which is an indicator of cell viability based on redox reactions: viable cells turn AquaBluer from its oxidized form (nonfluorescent, blue) to the reduced form (fluorescent, red), and thus the fluorescence intensity (FI) is proportional to the number of viable cells in the sample. The assay was done using AquaBluer at a 1:100 dilution in complete medium, according to the manufacturer's instructions, and the viability was quantified by measuring the FI at λ_{ex} = 540 nm, λ_{em} = 590 nm. The cell viability relative to the control (untreated cells) was calculated following Equation 6:

$$Cell\ viability\ (\%) = FI\ (cells + drug)\ \frac{FI\ (drug)}{FI\ (cells - culture\ medium)} x100 \qquad (6)$$

Hemolysis studies. Whole blood was obtained from buffy coats of healthy blood donors. In a 1.5 mL eppendorf tube, PBS in 3% w/v, 80 µL of erythrocyte suspension, and 80 µL of each SLNs

dispersion (120 µg/mL) were added. The solutions were incubated for 4 hours at 37 °C and centrifuged at 13800 rcf for 10 minutes at 4 ºC. Then, 80 µL of the supernatant were transferred to a 96-well plate, and absorbance at λ=558 nm was measured using a Synergy Biotek H1 Microtiter Plate Reader. As positive and negative control, PBS and 1% Triton X-100 in PBS were used, respectively. The percentages of hemolysis were calculated using Equation 7:

$$Hemolysis(\%) = \frac{A_{Sample}\ xA_{PBS}}{A_{Triton} xA_{PBS}} X100, \quad (7)$$

where A_{sample}, A_{PBS}, and $A_{Trtiton}$ are the absorbance of the sample, PBS and Triton respectively. The American Society for Testing and Materials International (ASTM) International protocol E2524-08, which considers: 0–2% non-hemolytic, 2–5% moderately hemolytic and >5% hemolytic, was followed.[49]

3. Results and discussion

As stated in the objectives (section 1.7), the aim of this work is the development of immunotheranostic formulations based on magnetic SLNs able to target and treat solid tumors. These formulations contain superparamagnetic iron oxide nanoparticles, which enable functionalities such as MRI and magnetic hyperthermia. In addition, the formulations carry immunomodulating drugs that disrupt the kynurenine signaling pathway, by inhibiting the IDO1 enzyme. To achieve these goals, we took a sequential synthetic approach, in which we prepared and thoroughly characterized each building block of the final assembled SLN prototypes.

3.1. SPIONs Synthesis and Characterization

Firstly, we synthesized the building blocks responsible for the MRI and magnetic hyperthermia functionalities of the formulations, i.e. the SPIONs. The magnetite (Fe_3O_4) nanoparticles were prepared using a co-precipitation method represented in Figure 2a). The synthesis of SPIONs using the co-precipitation method is convenient as it does not use organic solvents, is easy to perform, and produces oleic-acid coated NPs in high yield. Briefly, $FeCl_2 \cdot 4H2O$ and $FeCl_3 \cdot 6H2O$ were dissolved in water and a base (NH_4OH) was added to trigger the precipitation of magnetite[50] which was then coated with oleic acid to facilitate their encapsulation in the SLNs.

The morphology and size of the synthesized SPIONs were evaluated using TEM (Figure 2d), observing that the particles were roughly spherical, with a Gaussian distribution of sizes (Figure 2b) with an average diameter of 12 ± 3 nm (mean ± standard error of the mean, N = 300 SPIONs). We studied the crystalline structure of the particles using XRD (Figure 2c), denoting the presence of the inverse spinel structure, characteristic of the magnetite, with diffraction peaks in agreement with what was previously reported in the literature.[51] Altogether, these results confirm the absence of impurities and the success of the SPION synthesis, which were then used as a building block in the development of the immunotheranostic formulations of this project.

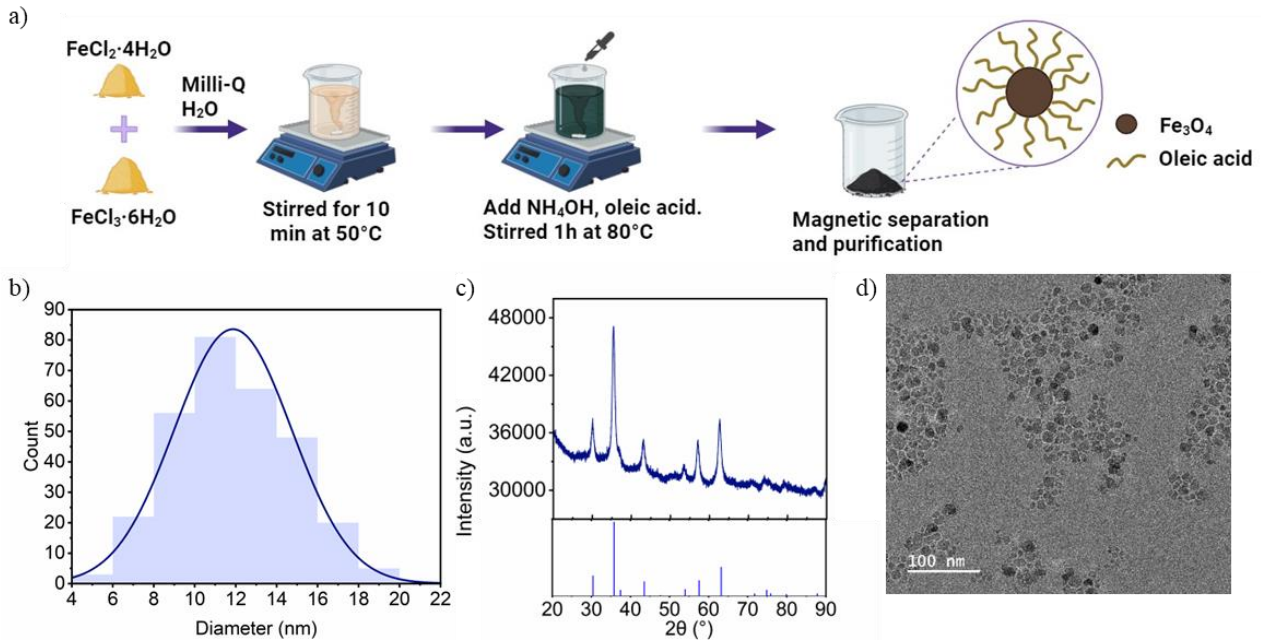

Figure 2. Synthesis and characterization of superparamagnetic iron oxide nanoparticles. a) Schematic representation of the synthesis protocol to obtain the iron oxide nanoparticles. b) Size distribution of iron oxide nanoparticles. c) XRD pattern of iron oxide nanoparticles showing the expected peaks for magnetite. Top: XRD pattern of iron oxide nanoparticles. Bottom: XRD pattern of magnetite (COD 1011032) d) Representative TEM images of iron oxide nanoparticles, showing spherical shape.

3.2.Functionalization of the lipidic ligand DPPE

Following the synthesis of the SPIONs, we synthesized the building block responsible for the targeting capabilities of the formulation. The surface of the SLNs was functionalized for it to be specific for solid tumors that overexpress the IDO1 enzyme, which is responsible for a higher rate of conversion of Trp in kynurenine.[12] Hence, the aminoacid Trp was selected as the targeting moiety, and the lipid DPPE was chosen as the anchoring between the Trp and the SLN's surface. For the reaction of DPPE with Trp, an EDC/NHS reaction shown in Figure 3 was performed. The EDC/NHS reaction is fast and takes place at room temperature, allowing the conversion of the carboxylic group of the Trp into an effective leaving group. Since Trp contains a good leaving group, it reacts efficiently with the amino group of the DPPE and this results in the DPPE functionalized with Trp.

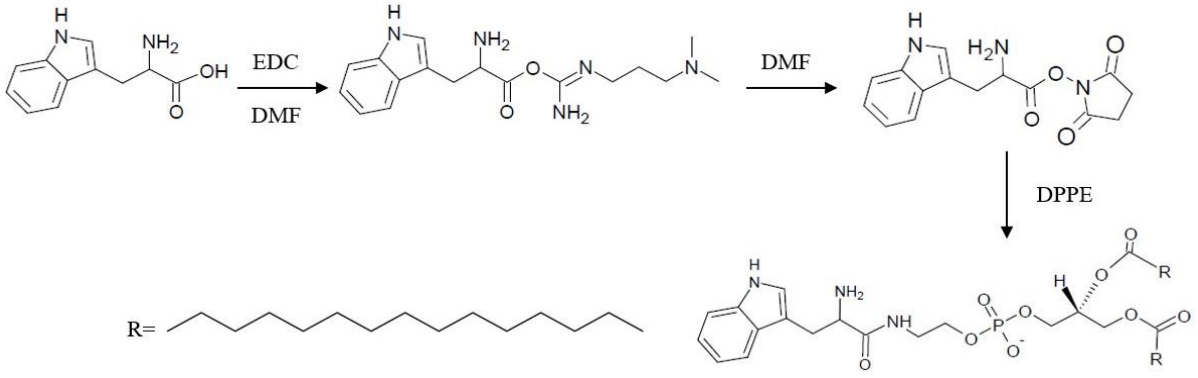

Figure 3: EDC-NHS reaction for the functionalization of SLNs. The carboxylic group of the Trp is first converted into an effective leaving group. Then, Trp reacts with DPPE.

We used an indirect method to calculate the yield of the reaction between DPPE and Trp, where the amount of free Trp left in the solution after the reaction was determined by fluorescence detection. We found that 98.7% of the Trp reacted with the DPPE, hence the functionalization was successful, and the building block was used for the synthesis of the final SLNs.

3.3. Targeted theranostics SLNs assembly and characterization

The prototypes developed in this project are SLNs whose matrix and surfactant are carnauba wax and Tween 80®, respectively. These two components were selected for their biocompatibility and safety. For instance, carnauba wax is FDA-approved for use in food,[52,53] and the non-ionic surfactant Tween 80® is regarded as safe for use in pharmaceutical formulations.[54] The SLNs were synthesized using a modified melt-emulsification method described in previous protocols (Figure 4a).[55] This method uses ultrasonication to mix the organic and aqueous phases and obtain a stable water dispersion of wax nanoparticles, avoiding the employment of organic solvents. SLNs with increasing levels of complexity were synthesized using this method. First, *control SLNs*, without any further building blocks, and SLNs made of carnauba wax encapsulating SPIONs (*SLNs@SPIONs*) were synthesized. Then, we incorporated DPPE in the synthetic process (*DPPE-SLNs@SPIONs*). The final step was the functionalization of the surface with DPPE-Trp. Hence, the final SLN prototype consists of carnauba wax-based SLNs, encapsulating SPIONs, and functionalized on their surface with Trp via a DPPE ligand (*DPPE-Trp-SLNs@SPIONs*).

The iron content (encapsulated in the SLNs) was determined by ICP-OES and results are shown in Table 1. The iron content did not change in the different formulations, showing that a difference in the composition of the SLNs did not affect their ability to encapsulate magnetite NPs. The hydrodynamic diameter of the synthesized SLNs was evaluated using DLS and NTA and the results are shown in Table 1.

Table 1. physicochemical properties of SLNs and Iron encapsulation efficiency

Formulation	D_h (DLS)	D_h (NTA)	Fe content
Control SLNs	240 ± 12 nm	190 ± 2 nm	-
SLNs@SPIONs	322 ± 49 nm	194 ± 2 nm	22 ± 3 %
DPPE-SLNs@SPIONs	223 ± 26 nm	180 ± 1 nm	23 ± 1 %
DPPE-Trp-SLNs@SPIONs	190 ± 13 nm	173 ± 4 nm	23 ± 1 %

The diameter obtained by DLS measurement was slightly higher than the one obtained by NTA. This is probably because for NTA a more diluted sample was used, reducing the possibility of aggregates or multiple scattering. Furthermore, NTA provides a number-weighted size, which differs from the intensity-weighted size obtained by DLS, which is highly influenced by the presence of large aggregates. Despite the difference in the results, both NTA and DLS showed an average size of around 200 nm for the different SLNs. The presence of SPIONs and the functionalization did not change significantly the size of the SLNs. The colloidal stability and PI of the SLNs were also characterized by DLS. The colloidal stability of the different SLNs was confirmed by ζ-potential, which oscillated from -40 mV to -35 mV for the different SLNs. As it is possible to observe in Figure 4d), the surface charge of the prototypes is negative and has a similar value. The presence of a negative ζ-potential was expected because of the presence of fatty acids in the carnauba wax. The functionalization was not expected to significantly influence the surface charge of the SLNs as a very small amount of ligand is present compared to the amount of wax (2.5% w/w). The PI of the different formulations is shown in Figure 4c). It did not exceed 0.25 and confirmed the presence of a homogeneous population. The morphology of the SLNs was

studied using TEM, confirming that the particles had a spherical shape and encapsulated the SPIONs, which were visible as dark spots inside the SLNs (Figure 4 e) to h)).

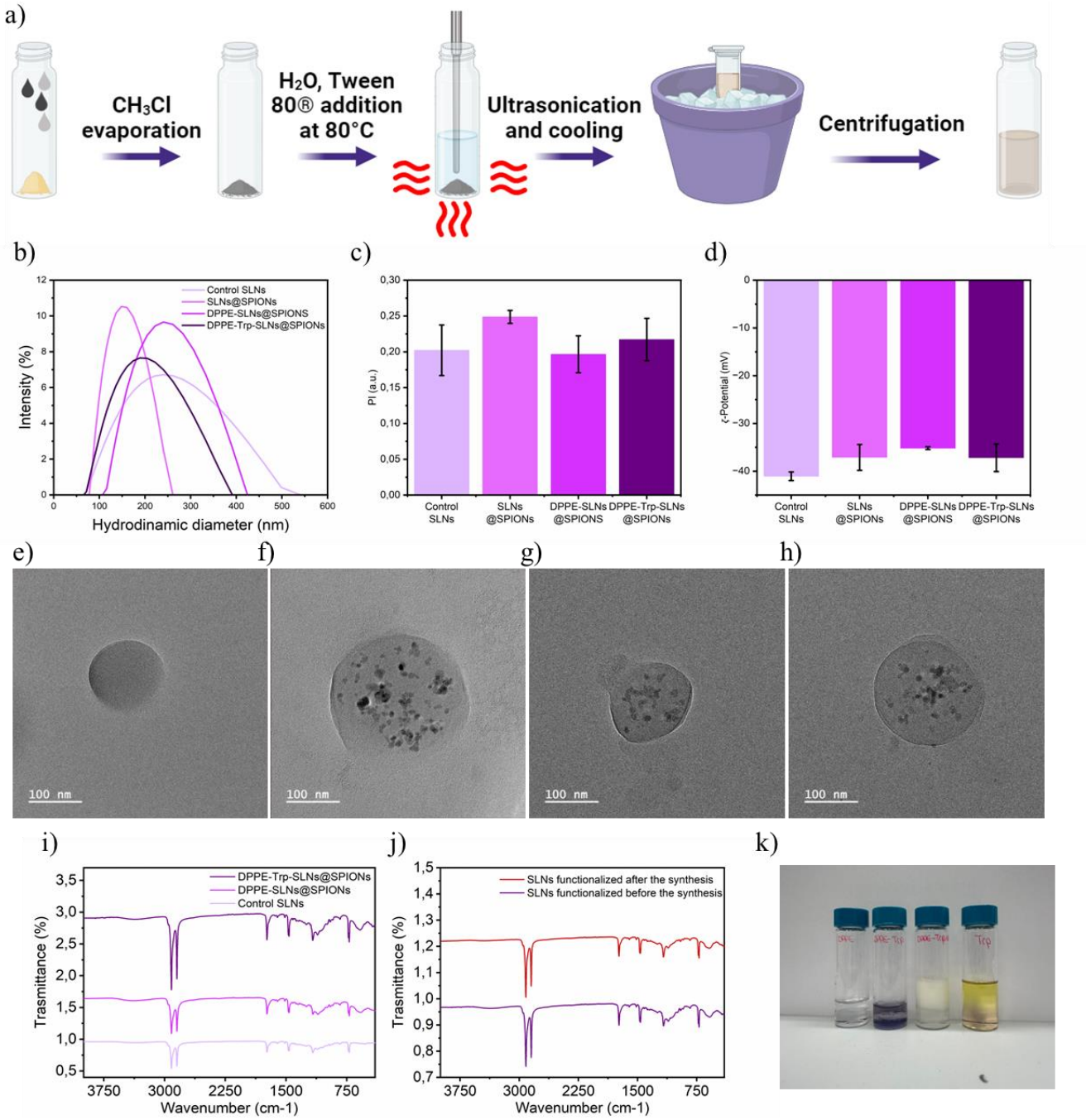

Figure 4. Synthesis and characterization of SLNs. a) Schematic representation of the synthesis protocol to obtain the SLNs. Plot of the evolution of b) the particles size. c) the PI d) the ζ-potential. Representative TEM images of e) control SLNs, f) SLNs@SPIONs, g) DPPE- SLNs@SPIONs, h) DPPE-Trp- SLNs@SPIONs. i) FTIR spectra of the different SLNs. j) comparison of the FTIR spectrum of the DPPE-Trp-SLNs@SPIONs functionalized before and after the syntesis. k) Hopkin's Cole test performed on (from left to right): a chloroform solution of DPPE; the chloroform solution of DPPE-Trp; the DPPE-Trp-SLNs; a ethanol solution of Trp.

After the spherical shape, the colloidal stability, and the homogeneity of the SLNs were confirmed, the success of the final SLNs' surface functionalization was investigated. To confirm the presence of DPPE and Tryptophan in the SLNs, FTIR analysis was used and the spectra are shown in Figure 4 i). However, probably due to the low concentration of DPPE and Trp, the characteristic peaks of these components were not visible in the spectrum of the final SLNs. Furthermore, DPPE is a lipid with bands close to the ones of the wax, which are difficult to

distinguish in the final particles. The presence of a large amount of wax compared to that of DPPE and Trp could be responsible for the difficulty in their detection by FTIR. To show the presence of Trp in the final SLNs, the Hopkin's Cole Test was performed (Figure 4 k)). According to the literature, the presence of Trp is easily detectable with this method, as the test solution will turn violet.[56] The following solutions were prepared: i) a chloroform solution of DPPE, as the negative control, ii) the chloroform solution of DPPE-Trp, iii) the DPPE-Trp-SLNs, iv) an ethanol solution of Trp, as the positive control. The vial containing the chloroform solution of DPPE-Trp and the one containing the ethanol solution of Trp turned violet, confirming the presence of Trp. However, the vial containing the DPPE-Trp-SLNs did not show a color change. This is probably due to the presence of a low percentage of Trp, which is distributed on the surface of the SLNs and does not react efficiently with the glyoxylic acid to give a purple product. However, the fact that the solution with the functionalized lipid turned violet showed that the reaction of DPPE with Trp happened, confirming the results obtained by fluorescence detection.

To study if the functionalization of the SLNs would be detectable using another approach, the functionalization of the DPPE after the synthesis of the SLNs was performed. Hence, the DPPE-SLNs@SPIONs were first synthesized and the EDC/NHS reaction was performed on the SLNs containing DPPE. The yield of the reaction was determined using fluorescence detection, and it was 94.5%. However, the FTIR spectrum and the Hopkins-Cole test did not give a different result than the previously synthesized DPPE-Trp-SLNs@SPIONs. A comparison of the FTIR spectra of the SLNs functionalized before and after the synthesis is shown in Figure 4j). Further analysis is needed to prove the presence of Trp in the final SLNs. Functionalizing the DPPE before the synthesis is advantageous as it has a higher yield and is faster. Furthermore, functionalizing the SLNs containing the drug after their synthesis could yield an undesired release of the drug in the solution during the functionalization reaction. Hence, even though the reaction of DPPE with Trp was confirmed for both routes, the DPPE-Trp formation was performed before the synthesis for the final SLNs. The SLNs described in this section were the carriers used in the final formulations, where they simultaneously incorporated SPIONs and immunomodulating drugs. The drug loading and release capacity, as well as their magnetic properties and ability to act as contrast agents in MRI and as heat-generating sources in magnetic hyperthermia, were studied.

3.4.Drug loading and release

The possibility of encapsulating immunomodulating drugs in the SLNs was investigated. Indoximod, Epacadostat, and Linrodostat have been selected as good candidates as they are drugs that already reached clinical trials and have shown efficacy in inhibiting the IDO1 enzyme.[10] Their encapsulation in the SLNs is expected to improve their half-life and bioavailability. The encapsulation of the drugs was studied in the DPPE-Trp-SLNs@SPIONs; different amounts of drugs were tested and the drug encapsulation efficiency was calculated using HPLC by calculating the amount of free drug left in solution. However, from the results obtained for the Linrodostat encapsulation, it was not possible to calculate the percentage of drug that was loaded into the SLNs. The peak attributed to the drug was subjected to a shift in the retention time after the encapsulation, as shown in Figure 5a) and 5b). This is probably due to the decomposition of the drug. To investigate this hypothesis, a vial containing an ultrasonicated solution of Linrodostat and one containing a heated solution of Linrodostat were analyzed and showed the same retention times as the calibration curve, confirming that the decomposition did not happen because of the synthesis process. A vial containing Linrodostat dissolved in the release medium was then prepared and incubated at 37°C for 24 hours, to study if the decomposition was due to the conditions of the release. However, the retention time did not change for the solution in PBS either. Hence, the amount of Linrodostat loaded in the SLNs was not possible to calculate, and further studies to understand the reason for the shift in the retention time are needed. The retention time of Epacadostat and Indoximod, on the other side, did not shift, and the drug loading for these two drugs is represented in Figure c). While SLNs with Epacadostat reached a high drug loading,

the Indoximod was not encapsulated as efficiently. This is probably due to the higher hydrophobicity of Epacadostat which is a fluorinated compound, showing higher affinity for the wax matrix. The more hydrophobic nature was confirmed by the higher retention times in HPLC. As the encapsulation of Indoximod reached a maximum of 60%, drug release studies have been performed only on the SLNs containing Epacadostat, which presented nearly 100% encapsulation efficiency.

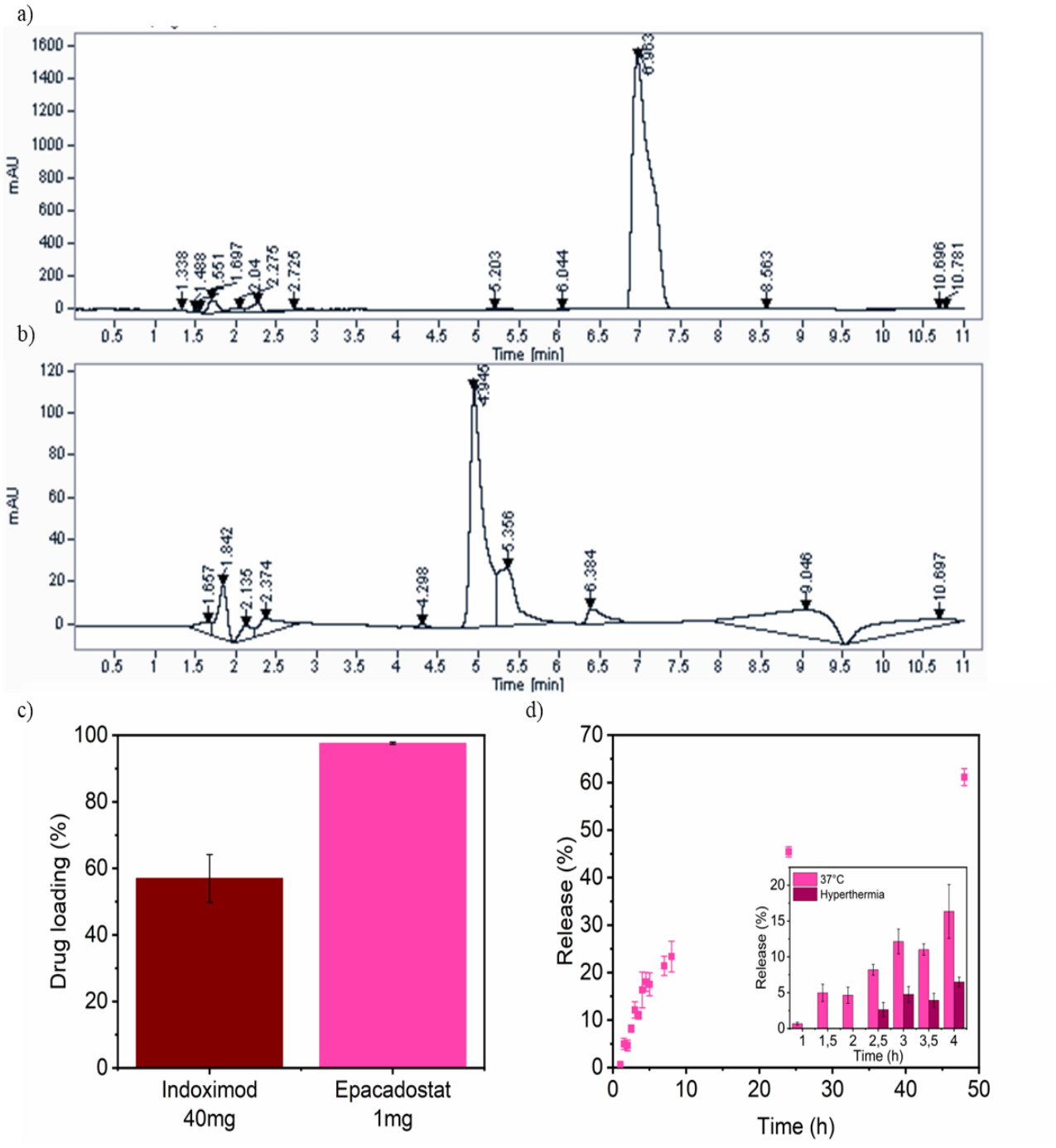

Figure 5. Drug loading and release. a) HPLC chromatogram of the highest concentration of the calibration curve for Linrodostat, showing a peak at retention time of 7 minutes. b) HPLC chromatogram for the Linrodostat encapsulation, showing a shift in retention time. c) bar plot for the loading of Indoximod and Epacasostat. b) Cumulative passive release of Epacadostat over 48h at room temperature. The inset is a comparison between passive and magnetic hyperthermia-induced release in the first 4h.

After determining the drug encapsulation efficiency, the release profile of Epacadostat was studied. The drug release was performed at 37°C in PBS + 1% Tween 80® up to 48 hours. A gradual release of the drug was observed, and it is shown in Figure 5d). The release reached only 23% after 8 hours and 60% after 48 hours. After 48 hours, however, the release did not reach a plateau yet. Hence, further studies on the release over a longer time are needed to better understand the kinetics of the drug release. Drug release under magnetic hyperthermia was performed to assess the effect of heat generation by the magnetic SLNs on their drug release profile. However, the drug release did not increase, which to a certain extent can be attributed to an insufficient Fe content in the SLNs to induce structural changes in the high melting temperature wax matrix that avoids an enhanced drug diffusion. Experimental parameters such as frequency and amplitude of the applied alternating magnetic field need to be optimized to achieve effective nanoscale temperature increases. A comparison between the first 4 hours of the release at 37°C and the release in hyperthermia is shown in the inset of Figure 5d). As no significant change was noticed after 4 hours, when hyperthermia was applied, the drug release in hyperthermia was not carried out for longer.

3.5. Magnetic characterization of theranostics SLNs

Magnetic characterization was performed on SLNs@SPIONs, DPPE-SLNs@SPIONs, and DPPE-Trp-SLNs@SPIONs. Hysteresis loops and T_2-weighted images were acquired to confirm the superparamagnetic behavior of the SPIONs inside the SLNs, the ability of the magnetic SLNs to act as magnetic hyperthermia effectors, and their efficiency as MRI contrast agents.

The magnetic properties of the SLNs were investigated using AC and DC magnetometry. DC magnetometry was performed to study if the superparamagnetic behavior of the SPIONs would be retained after encapsulation. As shown in Figure 6a), the hysteresis loops show quasi-null coercivity and remnant magnetization, demonstrating the superparamagnetic behavior of SPIONs both as free powder and when encapsulated in the SLNs. However, following the encapsulation, the magnetic saturation (M_s) was >15-fold lower. This result was expected as it is consistent with the fact that when the SPIONs are encapsulated in the SLNs, the non-magnetic wax contributes to the total mass of the sample. Interestingly, the magnetization curve for the DPPE-Trp-SLNs@SPIONs showed the lowest saturation magnetization, indicative of a higher non-magnetic mass contribution to the total mass that could be ascribed to the efficient further functionalization with Trp moieties on the SLNs' surface. AC measurements were performed to calculate the evolution of SAR values with the magnetic field. Different magnetic fields in the range of 4kA/m to 24 kA/m were applied while keeping constant the applied frequency (300 kHz). The result is a hysteresis loop that becomes broader when a higher magnetic field is applied. As the SAR value is obtained from the area of the hysteresis loops, the expected result was a linear increase of the SAR values with the magnetic field. The plot of SAR values versus the applied magnetic field is reported in Figure 6b). The values obtained are consistent with what was expected and show a linear correlation with the magnetic field.

The performance of the magnetic SLNs as T_2 contrast agents was tested at a preclinical magnetic field of 3T. T_2-weighted images and T_2 maps were acquired at different iron concentrations for SLNs@SPIONs, DPPE-SLNs@SPIONs, and DPPE-Trp-SLNs@SPIONs. All formulations demonstrated an iron concentration dependence transverse relaxation time (t_2) according to the T2-maps, shown in Figure 6c), indicating their potential as MRI contrast agents. From the T_2 maps, the relaxivity values were calculated and are shown in Figure 6e). Relaxivity values were obtained by plotting $1/t_2$ versus [Fe], which shows a linear correlation. The slope of the linear fitting corresponds to the relaxivity. In general, relaxivity values obtained for the different SLNs were slightly higher than the ones of FDA-approved contrast media such as Ferridex (93 mM^{-1} s^{-1}) and Resovist (143 mM^{-1} s^{-1}) measured in the same conditions.[57] A deeper analysis of the results shows a decrease of the transverse relaxivity (r2) for the SLNs-DPPE-Trp@SPIONs compared

to the non-functionalized SLNs@SPIONs and the functionalized SLNs-DPPE @SPIONs (133 vs 152 mM-1s-1 , respectively). This could be attributed to the SLNs' surface functionalization with Trp moieties, which would sterically hinder the water molecules' diffusion closer to the magnetic cores. Therefore, together with the magnetic results, this could additionally support the efficiency of the Trp functionalization on the SLNs' surface, which could not be proven by other characterization approaches. However, further analysis is needed to determine the error. High relaxivity values are important in MRI imaging as they reflect a better ability of the SLNs to modify the relaxation times of nearby water protons. Hence, the different SLNs were demonstrated to be suitable as MRI contrast agents.

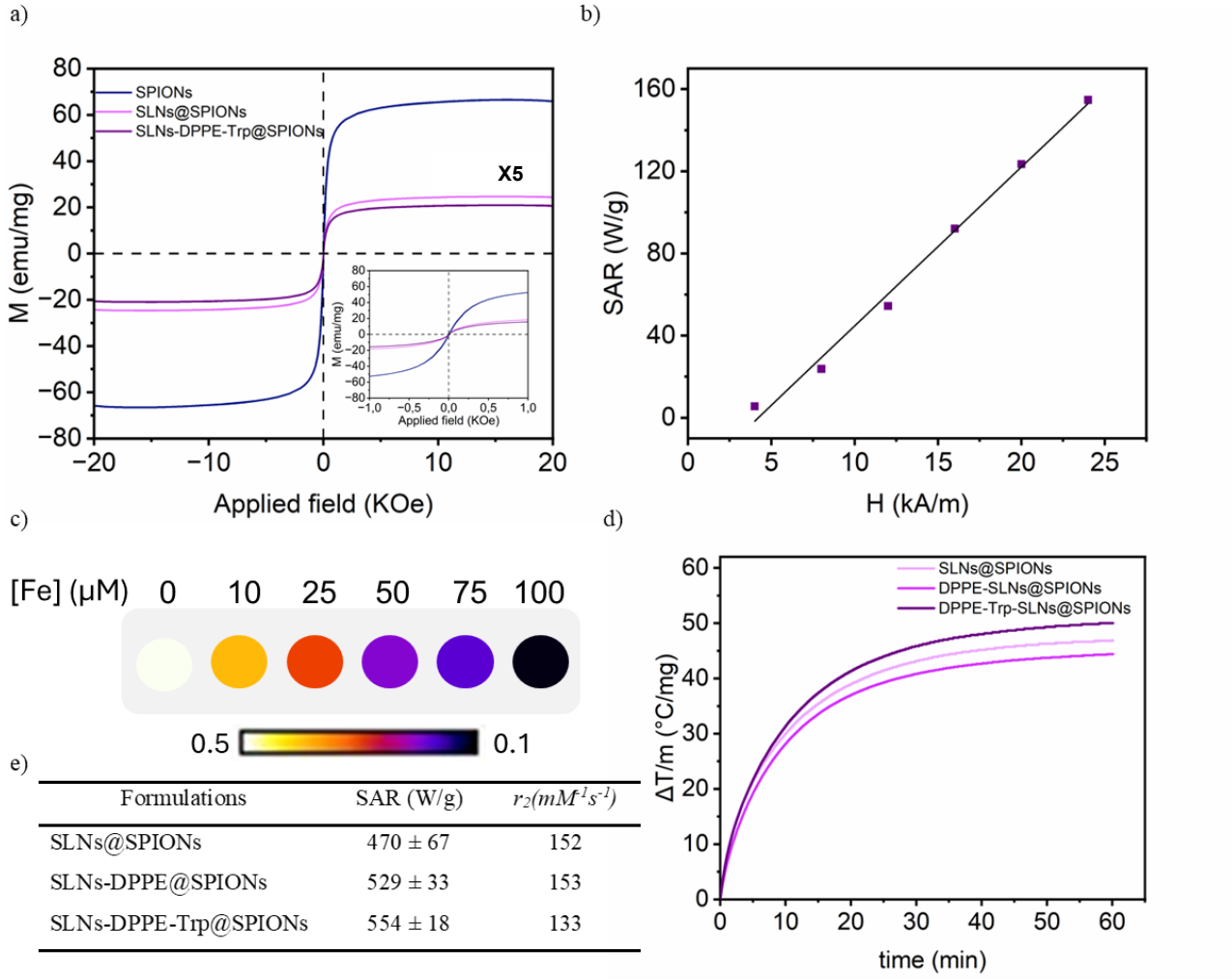

e)

Formulations	SAR (W/g)	$r_2(mM^{-1}s^{-1})$
SLNs@SPIONs	470 ± 67	152
SLNs-DPPE@SPIONs	529 ± 33	153
SLNs-DPPE-Trp@SPIONs	554 ± 18	133

Figure 6. Magnetic characterization of SLNs. a) Hysteresis loops of SPIONs, SLNs@SPIONs, and DPPE-Trp-SLNs@SPIONs in the range of -20 to +20 kOe at room temperature. The magnetization values of the SLNs were multiplied by 5 to obtain a visible curve in the graph. Inset: zoom of the hysteresis loops in the low magnetic field region. b) Linear correlation of the SAR values vs the applied magnetic field for DPPE-Trp-SLNs@SPIONs in the range of 4 kA/m to 24 kA/m at the applied frequency of 300 kHz c) T_2-map phantom images of different dilutions of DPPE-Trp-SLNs@SPIONs, showing the dependence of the MRI relaxation time on the Fe concentration. d) Heating curves of SLNs@SPIONs, DPPE-SLNs@SPIONs, and DPPE-Trp-SLNs@SPIONs. e) SAR and r_2 values for SLNs@SPIONs, DPPE-SLNs@SPIONs, and DPPE-Trp-SLNs@SPIONs at applied frequency of 869 MHz and applied magnetic field of 200 Oe.

The efficiency of the SLNs as magnetic hyperthermia effectors was studied thorugh inductive heating studies. 500µl of dispersions containing SLNs@SPIONS, DPPE-SLNs@SPIONs, and DPPE-Trp-SLNs@SPIONs were used to test the ability of the SPIONs to increase the temperature of the water solution under the influence of an external alternating magnetic field. From the inductive heating studies, the heating profiles were obtained. A magnetic field of 200 Oe and a

frequency of 869 MHz were applied and the heating behavior of the SLNs was observed for one hour. As expected, as shown in Figure 6d), the temperature of the mixture increased significantly. This demonstrated that even though hyperthermia was not able to boost the release of immunomodulating drugs, it can still be used for increasing the temperature in the proximity of cancer cells, causing irreversible damage and apoptosis, when the experimental conditions of frequency and intensity are optimized. From the heating profiles of the SLNs, SAR values were then calculated using Equation 5 and are shown in Figure 6e). The SLNs demonstrated a high heating ability compared to FDA-approved formulations such as Feride (115 W/g) and Resovist (104 W/g), measured at similar magnetic fields and frequencies.[58] The SAR values of the SLNs highlight their potential as promising tools for magnetic hyperthermia.

3.6.Cell studies

After an in-depth characterization of the formulations and the assessment of their potential in cancer therapy, these formulations were found to be promising candidates for further development. Studies were performed to study the toxicity of the nanoparticles. The biocompatibility of the unloaded SLNs was first studied, to observe if the nanocarrier would have toxic effects on cells. SLNs control, SLNs@SPIONs, DPPE-SLNs@SPIONs, DPPE-Trp-SLNs@SPIONs at different concentrations (from 0 to 120 μg/mL) were incubated for 48 hours with peripheral blood mononuclear cells, dermal fibroblasts, breast cancer (H_s578T), and pancreatic cancer (MIA-PACA-2). After 48 hours, no toxic effects were visible as shown in Figure 7a). Hence, the SLNs are safe and do not damage blood mononuclear cells, dermal fibroblasts, breast cancer, and pancreatic cancer cells tested in this study, even at high concentrations. Then, the cytotoxicity of SLNs with Epacadostat was tested on the same cells and compared to the free drug. In this case, DPPE-Trp-SLNs@SPIONs with and without drug were incubated for 48 hours with peripheral blood mononuclear cells, dermal fibroblasts, and breast cancer (H_s578T). Results are shown in figure 7b). No toxicity was observed for the free drug nor for the SLNs, even at high concentrations. This was expected as Epacadostat is a IDO1 inhibitor, whose goal is not damaging cancer cells, but blocking the depletion of Trp and activating the immune system against cancer. Further studies are needed to assess whether the encapsulation can improve the drug internalization into the cancer cells. Nowadays, Epacadostat demonstrated efficacy *in vitro*, but its capability of extending the lifetime of patients without disease progression is still limited.[17] We expect the SLNs to be an efficient nanocarrier, that could improve the tumor drug accumulation of Epacadostat and its efficacy *in vivo*. Once the toxicity of the nanoparticles was investigated, hemolysis studies were performed to study the cytotoxic effect of the SLNs on red cells. According to the ASTM protocol, a formulation is considered hemolytic when the percentage of hemolysis calculated by absorbance is higher than 5%. Control SLNs, SLNs@SPIONs, DPPE-SLNs@SPIONs, DPPE-Trp-SLNs@SPIONs at 120 μg/mL were first tested and the results are shown in Figure 7c). As can be observed, the SLNs control showed a higher percentage of hemolysis compared to the other formulations. This is probably due to interference from suspended particles in the solution, which changed the absorbance, giving a high value of hemolysis. Importantly, the final SLN did not show high values of hemolysis and we could proceed by investigating the formulations loaded with Epacadostat. Different concentrations of Epacadostat were tested: 10, 50, and 100 nM and results are shown in Figure 7d). No hemolysis was observed for low concentrations, but an increase was observed for the 100 nM concentration, for which, however, no critical level was reached. Hence, from the cell studies, it is possible to conclude that the formulations, both the nanocarrier alone and the one loaded with the drug, are safe and do not cause hemolysis, even at high concentrations. Further studies are needed to prove that the nanocarriers can enhance drug internalization in cancer cells, improving the therapeutic performance of Epacadostat.

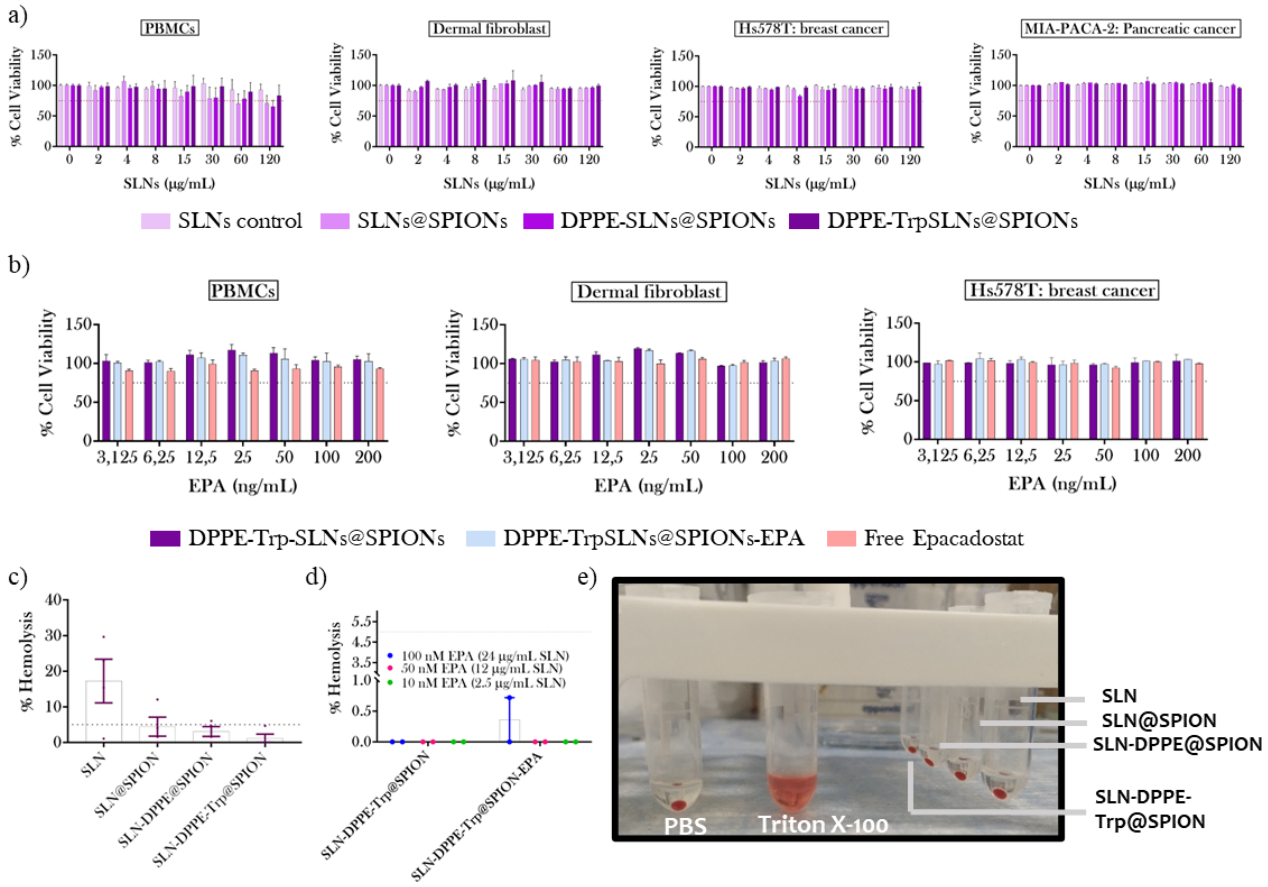

Figure 6. Cell studies. a) viability studied of Peripheral Blood Mononuclear Cell (PBMCs), dermal fibroblasts, breast cancer, and pancreatic cancer for unloaded SLNs in the range 0-120µg/mL. b) viability studied of Peripheral Blood Mononuclear Cell (PBMCs), dermal fibroblasts, and breast cancer for SLNs loaded with Epacadostat in the range 3-200 ng/mL. c) Hemolysis studies on unloaded SLNs, showing no hemolysis for all the formulations except for control SLNs. d) Comparison on hemolysis studies at different concentrations for DPPE-Trp-SLNs@SPIONs unloaded and loaded with Epacadostat. e) hemolysis studies on SLNs. PBS: negative control; Triton X-100: positive control; SLNs showing no hemolysis.

4. Conclusions and perspectives

Cancer immunotherapy is a growing field that has the potential to revolutionize cancer treatment by using an alternative approach to traditional therapies. The activation of the immune system against cancer cells is a promising substitute/complement for chemotherapy and surgery, which nowadays are the most effective ways of defeating cancer. Major developments in this area are the inhibition of immune checkpoints like PD-1 or enzymes such as IDO1. IDO1 is an enzyme that is overexpressed in some type of cancer and that is responsible for immune evasion. The depletion of Trp and the formation of kynurenine metabolites caused by the overexpression of IDO1 deactivates T-cells, which are fundamental in the immune response. Therefore, targeting IDO1 is a promising approach for activating the immune system against cancer minimizing the damage to healthy tissues.

In this work, we prepared targeted immunotheranostic formulations based on magnetic SLNs. The developed SLN formulations were synthesized using a modified melt-emulsification method and fully characterized using DLS, NTA, and TEM. The nanoparticles were homogeneous, with a spherical shape, and demonstrated colloidal stability. The surface of the SLNs was functionalized with Trp molecules, used as targeting ligands for cancer cells overexpressing IDO1. Magnetite nanoparticles were encapsulated for theranostic purposes. The magnetic properties of the SLNs were characterized using magnetometry, inductive heating, and MRI. Results showed that the formulations are promising for applications as T2-contrast agents in MRI as heat nanosources in magnetic hyperthermia. Moreover, an IDO1 inhibitor was successfully encapsulated in the nanoparticles and gradually released. Tests on healthy and cancer cells demonstrated that the nanocarriers are safe and do not cause hemolysis.

Future investigations are necessary to complete this work. Further studies must be conducted to prove the presence of Trp on the surface of the SLNs, although magnetic and MRI results suggest this possibility. This can be achieved through analytical chemistry and functional *in vitro* studies, for example, by studying if the functionalized particles are better internalized in cancer cells overexpressing IDO1. Thermogravimetric analysis might be useful by correlating a particular mass loss contribution with the presence of Trp molecules. Future investigations are also needed to understand the drug release kinetics. For this, release studies over a few days or weeks must be performed. Moreover, further studies *in vitro* and *in vivo* are necessary to prove the efficacy of the formulations in treating and targeting cancer. Altogether, this will provide us with valuable insights for the advanced design of future generations of theranostic formulations for cancer therapy.

References

1. Brown JS, Amend SR, Austin RH, Gatenby RA, Hammarlund EU, Pienta KJ. Updating the Definition of Cancer. *Mol Cancer Res*. 2023;21(11):1142-1147. doi:10.1158/1541-7786.MCR-23-0411
2. Bray F, Laversanne M, Sung H, et al. Global cancer statistics 2022: GLOBOCAN estimates of incidence and mortality worldwide for 36 cancers in 185 countries. *CA Cancer J Clin*. 2024;74(3):229-263. doi:10.3322/caac.21834
3. Kitsios K, Sharifi S, Mahmoudi M. Nanomedicine Technologies for Diagnosis and Treatment of Breast Cancer. *ACS Pharmacol Transl Sci*. 2023;6(5):671-682. doi:10.1021/acsptsci.3c00044
4. Zhang N, Zhou J, Li S, et al. Advances in Nanoplatforms for Immunotherapy Applications Targeting the Tumor Microenvironment. *Mol Pharm*. 2024;21(2):410-426. doi:10.1021/acs.molpharmaceut.3c00846
5. Youden B, Jiang R, Carrier AJ, Servos MR, Zhang X. A Nanomedicine Structure-Activity Framework for Research, Development, and Regulation of Future Cancer Therapies. *ACS Nano*. 2022;16(11):17497-17551. doi:10.1021/acsnano.2c06337
6. Hanahan D, Weinberg RA. Hallmarks of cancer: The next generation. *Cell*. 2011;144(5):646-674. doi:10.1016/j.cell.2011.02.013
7. Shao K, Singha S, Clemente-casares X, Tsai S, Yang Y. Nanoparticle-Based Immunotherapy. 2015;(1):16-30.
8. Zang X, Zhao X, Hu H, Qiao M, Deng Y, Chen D. Nanoparticles for tumor immunotherapy. *Eur J Pharm Biopharm*. 2017;115:243-256. doi:10.1016/j.ejpb.2017.03.013
9. Li J, Zeng H, Li L, Yang Q, He L, Dong M. Advanced Generation Therapeutics: Biomimetic Nanodelivery System for Tumor Immunotherapy. *ACS Nano*. 2023;17(24):24593-24618. doi:10.1021/acsnano.3c10212
10. Prendergast GC, Malachowski WP, DuHadaway JB, Muller AJ. Discovery of IDO1 Inhibitors: From bench to bedside. *Cancer Res*. 2017;77(24):6795-6811. doi:10.1158/0008-5472.CAN-17-2285
11. van der Zanden SY, Luimstra JJ, Neefjes J, Borst J, Ovaa H. Opportunities for Small Molecules in Cancer Immunotherapy. *Trends Immunol*. 2020;41(6):493-511. doi:10.1016/j.it.2020.04.004
12. Opitz CA, Somarribas Patterson LF, Mohapatra SR, et al. The therapeutic potential of targeting tryptophan catabolism in cancer. *Br J Cancer*. 2020;122(1):30-44. doi:10.1038/s41416-019-0664-6
13. Li L, Yang Z, Chen X. Recent Advances in Stimuli-Responsive Platforms for Cancer Immunotherapy. *Acc Chem Res*. 2020;53(10):2044-2054. doi:10.1021/acs.accounts.0c00334
14. Costa Da Silva M, Vieira Rocha C, Bañobre-López M, Gallo J. Stimulation and Suppression of the Innate Immune System through Nanotechnology. *ACS Appl Nano Mater*. 2021;4(3):2303-2316. doi:10.1021/acsanm.0c03424
15. Liu L, Pan Y, Zhao C, Huang P, Chen X, Rao L. Boosting Checkpoint Immunotherapy with Biomaterials. *ACS Nano*. 2023;17(4):3225-3258. doi:10.1021/acsnano.2c11691
16. Sun M, Yang S, Huang H, et al. Boarding Oncolytic Viruses onto Tumor-Homing Bacterium-Vessels for Augmented Cancer Immunotherapy. *Nano Lett*. 2022;22(12):5055-5064. doi:10.1021/acs.nanolett.2c00699
17. Cheng B, Yuan WE, Su J, Liu Y, Chen J. Recent advances in small molecule based cancer immunotherapy. *Eur J Med Chem*. 2018;157:582-598. doi:10.1016/j.ejmech.2018.08.028
18. Zakharia Y, McWilliams RR, Rixe O, et al. Phase II trial of the IDO pathway inhibitor indoximod plus pembrolizumab for the treatment of patients with advanced melanoma. *J Immunother Cancer*. 2021;9(6). doi:10.1136/jitc-2020-002057
19. Huynh JC, Cho M, Monjazeb A, et al. Phase I/II trial of BMS-986,205 and nivolumab as first line therapy in hepatocellular carcinoma. *Invest New Drugs*. 2024;42(1):35-43. doi:10.1007/s10637-023-01416-w
20. Mitchell MJ, Billingsley MM, Haley RM, Wechsler ME, Peppas NA, Langer R. Engineering precision nanoparticles for drug delivery. *Nat Rev Drug Discov*. 2021;20(2):101-124. doi:10.1038/s41573-020-0090-8
21. Morris EC, Neelapu SS, Giavridis T, Sadelain M. Cytokine release syndrome and associated neurotoxicity in cancer immunotherapy. *Nat Rev Immunol*. 2022;22(2):85-96. doi:10.1038/s41577-021-00547-6
22. Senapati S, Mahanta AK, Kumar S, Maiti P. Controlled drug delivery vehicles for cancer treatment and their performance. *Signal Transduct Target Ther*. 2018;3(1):1-19. doi:10.1038/s41392-017-0004-3
23. Paul W, Sharma CP. *Inorganic Nanoparticles for Targeted Drug Delivery*. Elsevier Ltd; 2019. doi:10.1016/B978-0-08-102680-9.00013-5
24. Mehnert W, Mäder K. Solid lipid nanoparticles: Production, characterization and applications. *Adv Drug Deliv Rev*. 2012;64(SUPPL.):83-101. doi:10.1016/j.addr.2012.09.021
25. Dal Magro R, Ornaghi F, Cambianica I, et al. ApoE-modified solid lipid nanoparticles: A feasible strategy to cross the blood-brain barrier. *J Control Release*. 2017;249:103-110. doi:10.1016/j.jconrel.2017.01.039
26. Tenchov R, Bird R, Curtze AE, Zhou Q. Lipid Nanoparticles from Liposomes to mRNA Vaccine Delivery, a Landscape of Research Diversity and Advancement. *ACS Nano*. 2021;15(11):16982-17015. doi:10.1021/acsnano.1c04996
27. Khan MI, Hossain MI, Hossain MK, et al. Recent Progress in Nanostructured Smart Drug Delivery Systems for Cancer Therapy: A Review. *ACS Appl Bio Mater*. 2022;5(3):971-1012. doi:10.1021/acsabm.2c00002
28. Chae J, Choi Y, Hong J, et al. Anticancer and Antibacterial Properties of Curcumin-Loaded Mannosylated Solid Lipid Nanoparticles for the Treatment of Lung Diseases. *ACS Appl Bio Mater*. Published online 2023. doi:10.1021/acsabm.3c01145
29. Shen MY, Liu TI, Yu TW, et al. Hierarchically targetable polysaccharide-coated solid lipid nanoparticles as an oral chemo/thermotherapy delivery system for local treatment of colon cancer. *Biomaterials*. 2019;197(September 2018):86-100. doi:10.1016/j.biomaterials.2019.01.019
30. Duan Y, Dhar A, Patel C, et al. A brief review on solid lipid nanoparticles: Part and parcel of contemporary drug delivery systems. *RSC Adv*. 2020;10(45):26777-26791. doi:10.1039/d0ra03491f
31. Bukhari SZ, Zeth K, Iftikhar M, et al. Supramolecular lipid nanoparticles as delivery carriers for non-invasive cancer theranostics. *Curr Res Pharmacol Drug Discov*. 2021;2(October):100067. doi:10.1016/j.crphar.2021.100067
32. Yasir M, Mishra R, Tripathi AS, et al. Theranostics: a multifaceted approach utilizing nano-biomaterials. *Discov Nano*. 2024;19(1). doi:10.1186/s11671-024-03979-w
33. Zhang H, Kang L, Zou Q, Xin X, Yan X. Coordination-assembled supramolecular nanoplatforms: structural modulation and theranostic applications. *Curr Opin Biotechnol*. 2019;58:45-52. doi:10.1016/j.copbio.2018.11.007

34. Stetefeld J, Mckenna SA, Patel TR. Dynamic light scattering : a practical guide and applications in biomedical sciences. *Biophys Rev*. Published online 2016:409-427. doi:10.1007/s12551-016-0218-6
35. Bhattacharjee S. DLS and zeta potential - What they are and what they are not? *J Control Release*. 2016;235:337-351. doi:10.1016/j.jconrel.2016.06.017
36. Filipe V, Hawe A, Jiskoot W. Critical evaluation of nanoparticle tracking analysis (NTA) by NanoSight for the measurement of nanoparticles and protein aggregates. *Pharm Res*. 2010;27(5):796-810. doi:10.1007/s11095-010-0073-2
37. ParticleMetrix GmbH. Introduction to Nanoparticles Tracking Analysis (NTA). Published online 2018:5. https://www.particle-metrix.de/fileadmin/pdf_technologien/TN_NTA_Introduction_EN.pdf
38. Inkson BJ. *Scanning Electron Microscopy (SEM) and Transmission Electron Microscopy (TEM) for Materials Characterization*. Elsevier Ltd; 2016. doi:10.1016/B978-0-08-100040-3.00002-X
39. Danino D. Cryo-TEM of soft molecular assemblies. *Curr Opin Colloid Interface Sci*. 2012;17(6):316-329. doi:10.1016/j.cocis.2012.10.003
40. Ismail AA, van de Voort FR, Sedman J. Chapter 4 Fourier transform infrared spectroscopy: Principles and applications. *Tech Instrum Anal Chem*. 1997;18(C):93-139. doi:10.1016/S0167-9244(97)80013-3
41. Epp J. *X-Ray Diffraction (XRD) Techniques for Materials Characterization*. Elsevier Ltd; 2016. doi:10.1016/B978-0-08-100040-3.00004-3
42. Van Geuns RJM, Wielopolski PA, De Bruin HG, et al. Basic principles of magnetic resonance imaging. *Prog Cardiovasc Dis*. 1999;42(2):149-156. doi:10.1016/S0033-0620(99)70014-9
43. Harvey D. ry ist em Ch yt ica l. *Anal Chem*. 2016;(2.1):6-7.
44. Iti S. ICP-OES: An Advance Tool in Biological Research. *Open J Environ Biol*. 2020;5:027-033. doi:10.17352/ojeb.000018
45. Padma Sree M. Vibrating Sample Magnetometer and Its Application In Characterisation Of Magnetic Property Of The Anti Cancer Drug Magnetic Microspheres. *Int J Pharm Drug Anal*. 2016;4(5):227-233.
46. Lemine OM. *Magnetic Hyperthermia Therapy Using Hybrid Magnetic Nanostructures*. Elsevier Inc.; 2019. doi:10.1016/B978-0-12-813906-6.00007-X
47. Rodrigo I, Castellanos-Rubio I, Garaio E, et al. Exploring the potential of the dynamic hysteresis loops via high field, high frequency and temperature adjustable AC magnetometer for magnetic hyperthermia characterization. *Int J Hyperth*. 2020;37(1):976-991. doi:10.1080/02656736.2020.1802071
48. Ma M, Zhang Y, Shen X, Xie J, Li Y, Gu N. Targeted inductive heating of nanomagnets by a combination of alternating current (AC) and static magnetic fields. *Nano Res*. 2015;8(2):600-610. doi:10.1007/s12274-015-0729-7
49. Dobrovolskaia MA, McNeil SE. Understanding the correlation between in vitro and in vivo immunotoxicity tests for nanomedicines. *J Control Release*. 2013;172(2):456-466. doi:10.1016/j.jconrel.2013.05.025
50. Kandasamy G, Maity D. Recent advances in superparamagnetic iron oxide nanoparticles (SPIONs) for in vitro and in vivo cancer nanotheranostics. *Int J Pharm*. 2015;496(2):191-218. doi:10.1016/j.ijpharm.2015.10.058
51. Mürbe J, Rechtenbach A, Töpfer J. Synthesis and physical characterization of magnetite nanoparticles for biomedical applications. *Mater Chem Phys*. 2008;110(2-3):426-433. doi:10.1016/j.matchemphys.2008.02.037
52. Food and Drug Administration. Food and drugs, Chapter 1- Food and Drug Administration Department of Health and Human Services, Subchapter B - Food for human consumption, Part 184 - Direct food substances affirmed as generally recognized as safe. 1994;1069(35):20656.
53. de Freitas CAS, de Sousa PHM, Soares DJ, da Silva JYG, Benjamin SR, Guedes MIF. Carnauba wax uses in food – A review. *Food Chem*. 2019;291(March):38-48. doi:10.1016/j.foodchem.2019.03.133
54. Kaur G, Mehta SK. Developments of Polysorbate (Tween) based microemulsions : Preclinical drug delivery , toxicity and antimicrobial applications. *Int J Pharm*. 2017;529(1-2):134-160. doi:10.1016/j.ijpharm.2017.06.059
55. García-Hevia L, Casafont Í, Oliveira J, et al. Magnetic lipid nanovehicles synergize the controlled thermal release of chemotherapeutics with magnetic ablation while enabling non-invasive monitoring by MRI for melanoma theranostics. *Bioact Mater*. 2022;8(October 2020):153-164. doi:10.1016/j.bioactmat.2021.06.009
56. Nurit E, Tiessen A, Pixley K V., Palacios-Rojas N. Reliable and inexpensive colorimetric method for determining protein-bound tryptophan in maize kernels. *J Agric Food Chem*. 2009;57(16):7233-7238. doi:10.1021/jf901315x
57. Rohrer M, Bauer H, Mintorovitch J, Requardt M, Weinmann HJ. Comparison of magnetic properties of MRI contrast media solutions at different magnetic field strengths. *Invest Radiol*. 2005;40(11):715-724. doi:10.1097/01.rli.0000184756.66360.d3
58. Song Y, Li D, Lu Y, et al. Ferrimagnetic mPEG-b-PHEP copolymer micelles loaded with iron oxide nanocubes and emodin for enhanced magnetic hyperthermia-chemotherapy. *Natl Sci Rev*. 2020;7(4):723-736. doi:10.1093/NSR/NWZ201